Limnology and Oceanography
FLUIDS & ENVIRONMENTS

ORIGINAL ARTICLE

The role of hydrodynamics in structuring in situ ammonium uptake within a submerged macrophyte community

Edward P. Morris,[1,2] Gloria Peralta,[1] Tom Van Engeland,[3] Tjeerd J. Bouma,[3] Fernando G. Brun,[1] Miguel Lara,[1] Iris E. Hendriks,[4] Javier Benavente,[1] Karline Soetaert,[3] Jack J. Middelburg,[3,5] and J. Lucas Perez-Llorens[1]

Abstract

In low-nutrient, macrophyte-dominated coastal zones, benthic ammonium (NH_4^+) uptake may be influenced by the structural properties of plant canopies via their effect on near-bed hydrodynamics. Using a dual-tracer (uranine and $^{15}NH_4^+$) method that does not require enclosures, we examined how this process affects nutrient uptake rates within a tidally dominated, patchy Caulerpa prolifera – Cymodocea nodosa *landscape. NH_4^+ uptake was determined by calculating tissue ^{15}N excesses and correcting for ^{15}N enrichment as derived from uranine concentration. Vertical hydrodynamic profiles were measured in the downstream flow direction from outside to inside of the* C. nodosa *bed by using an array of acoustic Doppler velocimeters. The transition from a* C. prolifera *to a* C. nodosa *bed included a change in both benthic canopy properties (short and dense to tall and sparse) and sediment topography (0.2-m increase in water column depth) that resulted in an increase in longitudinal advection and turbulent diffusivity within the* C. nodosa *canopy between 0.5 and 1.5 m from the leading edge. Vertical differences in canopy water exchange appeared to explain variations in uptake between biotic functional groups; however, no clear differences in longitudinal uptake were found. Using in situ labeling, this study demonstrated for the first time the role of hydrodynamics in structuring NH_4^+ uptake within an undisturbed, patchy macrophyte landscape.*

Keywords: nutrients, water flow, patchiness, *Cymodocea nodosa*, *Caulerpa prolifera*, $^{15}NH_4$

[1]Faculty of Marine and Environmental Sciences, University of Cádiz, 11510 Puerto Real, Spain

[2]Present address: Department of Ecology and Coastal Management, Instituto de Ciencias Marinas de Andalucía, Consejo Superior de Investigaciones Científicas, 11519 Puerto Real, Spain

[3]Centre for Estuarine and Marine Ecology, Netherlands Institute of Ecology, 4400 AC Yerseke, the Netherlands

[4]Instituto Mediterraneo de Estudios Avanzados, Universidad de las Islas Baleares y el Consejo Superior de Investigaciones Científicas, 07190 Esporles, Spain

[5]Faculty of Geosciences, Utrecht University, 3508 TA Utrecht, the Netherlands

Correspondence to Edward P. Morris, edward.morris@csic.es

Introduction

[1] Ammonium (NH_4^+) uptake by submerged macrophyte communities is a major pathway by which nitrogen is removed from the water column and potentially retained within shallow, marine, benthic ecosystems (Wallentinus 1984; Touchette and Burkholder 2000; Fernandes et al. 2009). The high foliar NH_4^+ uptake capacity of many marine angiosperms (Touchette and Burkholder 2000; Rubio et al. 2007; Alexandre et al. 2011) and macroalgae (O'Brien and Wheeler 1987; Vergara et al. 1997; Malta et al. 2005) indicates that, in systems with low-to-moderate nutrient concentrations, uptake is often controlled by rates of transfer across concentration boundary layers, rather than by enzymatic processes (Bilger and Atkinson 1992). Hence, an increase in NH_4^+ concentration

Limnology and Oceanography: Fluids and Environments • 3 (2013): 210–224 • DOI 10.1215/21573689-2397024

or water velocity strongly enhances macrophyte uptake (Hurd et al. 1996; Thomas et al. 2000; Koch et al. 2006).

[2] Macrophyte communities often form distinctly patchy distributions consisting of bare and vegetated areas as well as patches of different species. Water flow interacts with these patchy landscapes, resulting in horizontal (Fonseca and Koehl 2006) and vertical (Gambi et al. 1990; Ackerman and Okubo 1993; Koch and Gust 1999) differences in water velocity and turbulence that influence NH_4^+ uptake rates of individual canopy elements (Cornelisen and Thomas 2002; Morris et al. 2008). That is, the physical interaction of macrophyte structures with water movement results in spatially structured variation in benthic NH_4^+ transport rates. Furthermore, intra- and interspecific differences in macrophyte canopy properties, such as canopy morphology (Verduin and Backhaus 2000; Stewart and Carpenter 2003; Hendriks et al. 2010), the density of elements (Fonseca et al. 1982; Peterson et al. 2004; Lacy and Wyllie-Echeverria 2011), stiffness (Gaylord and Denny 1997; Bouma et al. 2005; Peralta et al. 2008), and patchiness (Folkard 2005; Maltese et al. 2007), strongly influence near-bed flow properties. Consequently, macrophyte landscapes potentially have a wide range of nutrient transport niches determined solely by physical interactions with water flow.

[3] Simple canopy structure metrics, such as the diameter (d) and density of structures (n), projected frontal area per unit volume ($a = nd$), canopy height (h_c), and the canopy drag coefficient ($C_D \sim 1$), can help to anticipate these interactions (Nepf and Ghisalberti 2008; Ghisalberti and Nepf 2009). In sparse canopies ($ah < 0.04$, where h = height), the vertical water velocity profile is that of a rough boundary layer with notable within-canopy longitudinal advection over a transition length scale (L_T), which may be larger than the patch length (Ghisalberti and Nepf 2009). In dense canopies ($ah > 0.3$), the extent of vortex penetration into the canopy (δ_e) and L_T are proportional to the drag length scale of the canopy, $(C_D a)^{-1}$, and at longitudinal distances exceeding L_T, exchange is dominated by Kelvin–Helmholtz vortices (Nepf and Ghisalberti 2008). For very dense canopies, δ_e is very small ($\sim 2d$), and the majority of canopy exchange is controlled by stem-scale turbulence (White and Nepf 2008). Hence, the relevant hydrodynamic regime that controls canopy water exchange (and potential nutrient supply) can be very different, depending on a species' structural characteristics.

[4] Differences in the relevant hydrodynamic regime controlling canopy nutrient exchange may be expected within subtidal *Caulerpa prolifera–Cymodocea nodosa* landscapes, which are made up of two very different canopy types. *C. prolifera*, a rhizophytic, soft-sediment dwelling alga, forms extensive, short ($h_c \sim 0.05 - 0.13$ m) and dense canopies ($a > 100\ m^{-1}$) that often surround patches of tall ($h_c \sim 0.2 - 1$ m), relatively sparse ($a \sim 1 - 5\ m^{-1}$) *C. nodosa*, a marine angiosperm. We estimate that L_T is in the order of 0.02 m for *C. prolifera* and 5 m for *C. nodosa*; that is, longitudinal flow penetrates ~250 times farther into the *C. nodosa* than the *C. prolifera* canopy. Furthermore, as *C. prolifera* $(ah)^{-1}$ is generally $<< 2d$, δ_e/h is expected to be small (White and Nepf 2008), suggesting low rates of vertical water exchange. In contrast, for *C. nodosa*, canopy water exchange is expected to be dominated by a mix of longitudinal advection and vertical diffusivity associated with Kelvin–Helmholtz vortices. In other words, both longitudinal water flow and mixing are predicted to be much larger in the *C. nodosa* than in the *C. prolifera* canopy. As water flows over the upstream–downstream transition between the dense *C. prolifera* and sparse *C. nodosa* canopies, because of the difference in canopy density, a transition in the shape of the vertical velocity profile is predicted that results in a gradient of increasing near-bed water velocities across the transition. Furthermore, flow adjustment should be observable upstream of the leading edge of the *C. nodosa* canopy at a length scale comparable to the canopy height (Rominger and Nepf 2011), suggesting changes in flow properties at the transition that extend into the *C. prolifera* bed. We hypothesized that if NH_4^+ uptake is physically limited, these changes in water flow properties will manifest as spatially explicit differences in the uptake rates of biota within the canopies.

[5] Few studies have examined how differences in hydrodynamics act to structure the ammonium uptake of natural benthic macrophyte communities. Traditionally, NH_4^+ uptake rates are measured using a chamber

(Thursby and Harlin 1982; Hemminga et al. 1994; Naldi and Viaroli 2002), in which hydrodynamic conditions and the structure of macrophyte communities deviate strongly from natural conditions. Flow chambers that generate both unidirectional and oscillatory currents allow the preservation of hydrodynamic effects (Thomas and Atkinson 1997; Thomas et al. 2000; Thomas and Cornelisen 2003) and, when combined with stable-isotope labeling, allow the contributions of individual macrophyte community components to be assessed with minimal disturbance to canopy structure (Cornelisen and Thomas 2002; Cornelisen and Thomas 2004; Lepoint et al. 2007). Nevertheless, although crucial to the development of modeling approaches (Falter et al. 2004; Cornelisen and Thomas 2009), these studies are a simplification of natural systems; they usually require the transplantation of macrophyte communities or the use of a field flume with spatial dimension inappropriate for examining heterogeneous landscapes.

[6] An alternative is stable-isotope labeling without enclosures, which has been applied successfully in a number of aquatic systems (Hughes et al. 2000; Gribsholt et al. 2005; Pace et al. 2007). Based on these principles, we devised a system that allowed us to spike the water column over a shallow, submerged *Caulerpa prolifera–Cymodocea nodosa* landscape with a mix of $^{15}NH_4^+$ and uranine (an Na salt of fluorescein). By measuring the spatial distribution of uranine and the incorporation of $^{15}NH_4^+$ within plant tissues, we examined in situ NH_4^+ uptake rates of the natural phototrophic community under undisturbed hydrodynamic conditions. Using this technique, we examined the hypothesis that spatial differences in hydrodynamics influence in situ NH_4^+ uptake within an undisturbed natural, patchy macrophyte community.

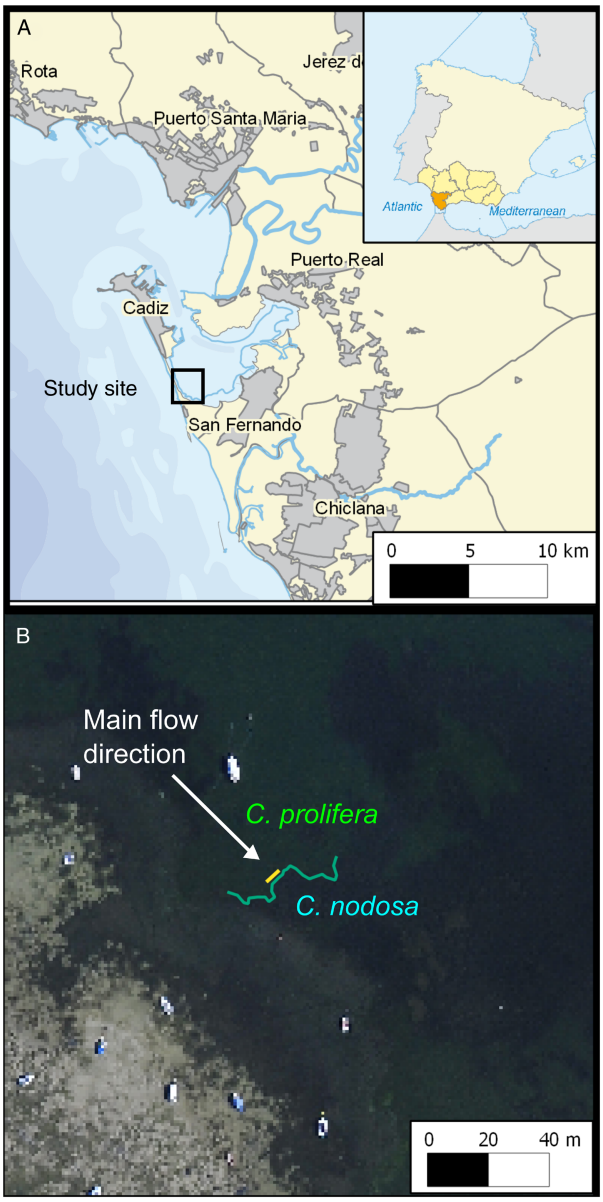

Fig. 1 Map of study location: Bay of Cádiz, southwestern Spain with insert of larger region (A), and airborne photograph of the *Caulerpa prolifera–Cymodocea nodosa* boundary (B), with the patch boundary highlighted in blue and the position of the nutrient delivery system in yellow. Visualization of aerial photographs (kindly supplied by L. Del Río Rodríguez, University of Cádiz) was carried out by using QGIS (www.qgis.org).

Methods

Study Site

[7] Labeling experiments were carried out in Cádiz Bay located in the west of the Gulf of Cádiz, southwestern Spain, between 36° 23′ and 36° 37′ N latitude and between 6° 8′ and 6° 15′ W longitude (Fig. 1A). The bay is divided into two basins, a shallower basin (inner bay) with a mean depth of 3 m MLW (mean low water) (Freitas et al. 2008) and a deeper basin (outer bay) with a mean depth of 12 m MLW (Rueda and Salas 2003). The inner bay is protected from the action of large waves but is strongly influenced by semidiurnal co-oscillating tides with mean amplitude of 1.5 m (Alvarez et al. 2003).

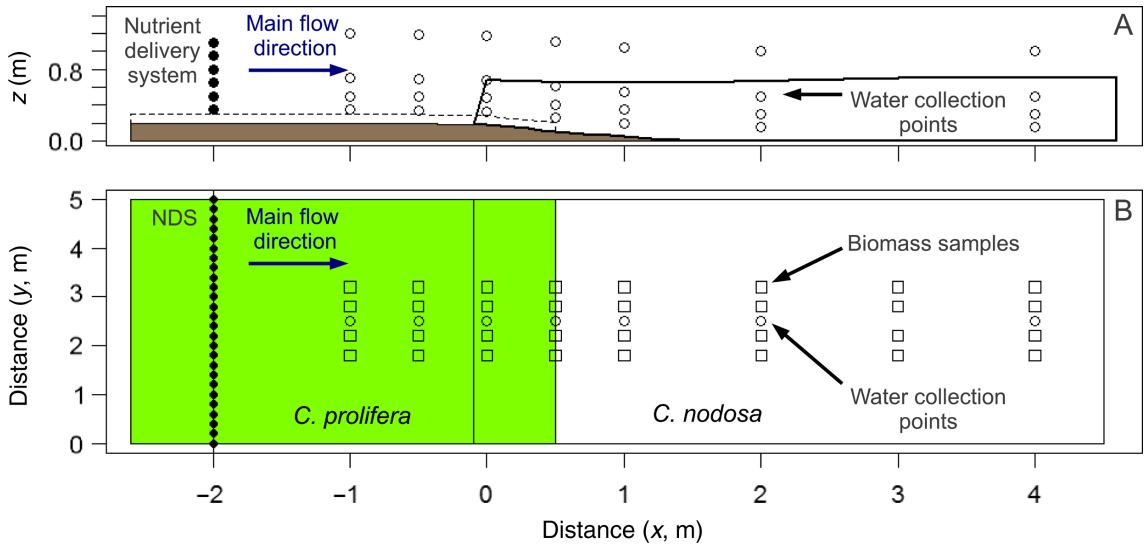

Fig. 2 Schematic $x-z$ (A) and $x-y$ (B) diagrams of the experimental design. Filled circles represent the release points of the nutrient delivery system (NDS); open circles, water collection points; and squares, biomass samples. Horizontal distance (x-axis, m) is relative to the edge of the *C. nodosa* patch and parallel to the main flow direction. The increase in the sediment surface height within the *C. prolifera* canopy (dashed line) is represented by a brown polygon. Water column height (z-axis, m) is relative to the sediment surface at $x = 2$ m within the *C. nodosa* canopy (represented by a solid line). The green polygon represents the extent of the *C. prolifera* bed.

[8] Experiments were carried out in the shallow (0.5 m lowest astronomical tide), southwestern region of the bay (Fig. 1A, Santibañez) where maximum free-stream current velocities range between 0.03 and 0.1 m s^{-1}. A 10-m-long, relatively straight section of a large macrophyte community dominated by a *Cymodocea nodosa* Ucria (Ascherson) patch bordered by a dense bed of *Caulerpa prolifera* (Forsskål) J.V. Lamouroux was chosen to examine the transition between canopy types (Fig. 1B). Previous hydrodynamic measurements showed that ~30 min after low tide, current direction was essentially unidirectional, parallel to the shore (x-direction), and perpendicular to the edge of the *C. nodosa* patch (y-direction). Sediment height (z_s) was not constant across the transition between the two species; the *C. prolifera* bed ($x = -1$ m) was 0.2 m higher than the *C. nodosa* bed ($x = 2$ m) (Fig. 2). We defined water column height (z) relative to the sediment surface at $x = 2$ m; however, we also refer to height (h) above the sediment surface. The experiment was carried out on 2 August 2007 at ~13:00 (UTC + 1) when $z = 1.35$ m; by the end of the release, $z = 1.53$ m. Photosynthetic photon flux measured using a custom data logger (Apogee SQ-100 sensor; Apogee Instruments, Inc., USA) connected to an Onset HOBO data logger (Onset Computer Corporation, USA) at $z = 0.5$ (within the *C. prolifera* bed) during the labeling period was 801 ± 95 μmol-quanta m^{-2} s^{-1} (mean ± standard error); water temperature was 27.7 ± 0.2 °C, and salinity, 34.

Canopy Properties

[9] Canopy structural properties for each species are shown in Table 1. The density and biomass of above-sediment structures were estimated by collecting all plant material within randomly selected 0.2×0.2–m quadrants ($n = 4$). Canopy height (h_c) was assessed by measuring the distance from the top of the canopy

Table 1 Summary of macrophyte canopy properties [range or mean ± SD (n)].

Property	*C. prolifera*	*C. nodosa*
Structure density (structures m^{-2})	8700 ± 146 (4)	356 ± 60 (4)
Leaves per shoot	—	3.5
Structure width (d, m)	0.03	0.006
Structure thickness (e, m)	1×10^{-3}	1×10^{-3}
Biomass (gDM m^{-2})	200 ± 13 (4)	258 ± 25 (4)
Canopy height (h, m)	0.1 ± 0.02 (5)	0.5–0.7 (8)
Frontal area of structures per water volume (a, m^{-1})	183	3.8
ah (dimensionless)	18.3	1.9–2.7
Canopy porosity (dimensionless)	0.87	0.996

(assessed by eye in situ) to the sediment surface at a number of positions haphazardly situated throughout the experimental area and calculating the arithmetic mean (i.e., equivalent to the average roughness height). h_c was relatively constant for *C. prolifera*, whereas for *C. nodosa* it varied between 0.5 m at the leading edge and 0.7 m at $x = 4$ m (Fig. 2). *C. nodosa* morphology (number of leaves, leaf length, width, and thickness) represents the mean values of samples collected in summer between 2005 and 2011 as part of a *C. nodosa* monitoring program (www.famar.wordpress.com). *C. prolifera* morphology was derived from Vergara et al. (2012). Vertical profiles of the frontal area of structures per water volume (a, m^{-1}) were calculated using a cumulative probability function of the distribution of structure lengths scaled to the in situ h_c. Unfortunately, *C. nodosa* epiphyte biomass was not quantified. Rather, summer biomass estimates of 0.18 ± 0.08 $gDM_{epiphytes}$ $gDM_{C.\ nodosa}$ ($n = 18$; P. García-Marin, University of Cádiz, pers. comm.) were used. Unattached macroalgae (*Gracilaria* sp.) were sparsely distributed within the lower canopy of the macrophyte beds.

Hydrodynamic Measurements

[10] Vertical profiles of hydrodynamic properties were measured in the downstream flow direction (x) from outside to inside of the *C. nodosa* patch (~5 m offshore from the nutrient delivery system [NDS]) by using four acoustic Doppler velocimeters (ADV; two Vector, one NDV, and one Vectrino, Nortek AS, Norway) fixed on a single frame at $x = -0.8$, 0, 0.7, and 1.5 m, perpendicular to the leading edge of the *C. nodosa* bed. Vertical profiles were collected by moving the frame by hand, up and down, cycling through heights of $z = 0.48$, 0.68, 0.88, 0.98, 1.08, and 1.28 m. ADV measurements were carried out over a 1-h time interval coinciding with the nutrient release. The ADV frame was left at each z-position for ~300 s before being moved to the next z-position, resulting in three measurement periods at $z = 0.48$ m, one at $z = 1.28$ m, and two at the remainder ($z = 0.68$–1.08 m). A single ADV also recorded water velocity and depth at a height of 0.5 m above the sediment surface in the *C. prolifera* bed.

[11] Velocity components (u, v, and w in the x-, y-, and z-directions, respectively) were measured at 25 or 64 Hz. Coordinates were rotated in the x–y plane so as to align u with the x-axis, correcting for slight variations in the orientation of the individual ADVs and the frame. All three velocity components with any of the individual beam correlations < 70% or signal-to-noise ratio < 5 were discarded. Velocity spikes were removed using the phase-space despiking algorithim in the free software package WinADV (Goring and Nikora 2002; Wahl 2003). Time-averaged velocity components ($\bar{u}$, $\bar{v}$, and $\bar{w}$) and their respective fluctuations (u', v', and w') were calculated by averaging the temporal measurements ($n = 2.5$–15×10^3) at each sampling point as described in Morris et al. 2008. $\bar{u}$ was fitted to a second-order polynomial surface to extract values corresponding to the positions of uptake measurements (see below). Because measurements were missing from the lower regions of both canopies, to aid the fitting procedure we inserted near zero (0.005 m s^{-1}) $\bar{u}$ values at midway within the *C. prolifera* canopy and just above the sediment surface in the *C. nodosa* canopy.

Turbulent Diffusivity Coefficients

[12] Turbulent diffusivity in the x-, y-, and z-directions, at each sampling point of the vertical profiles was derived from Taylor's theory according to Holtappels and Lorke (2011). Normalized autocorrelation coefficients of the root-mean-squared velocity fluctuations (u'_{RMS}, v'_{RMS}, and w'_{RMS}) were calculated for all time intervals (t) within each burst period (using the R function acf; http://www.r-project.org/). t values were translated into spatial distances (r) according to $r = t\bar{U}$, where $\bar{U}$ is the modulus of velocity (i.e., $\bar{u} + \bar{v} + \bar{w}$), transforming the autocorrelation coefficients into Eulerian spatial correlation coefficients (E_E). E_E was integrated over the spatial distance (r) (using the R function cumsum). The integral length scale (L_E) was defined as the first maximum of integrated E_E, which corresponds to the first zero crossing of the autocorrelation coefficient. Turbulent diffusivity coefficients derived from Taylor's theory (K, m^2 s^{-1}) were calculated as the product of the root-mean-squared velocity deviation and L_E

for each direction, respectively (e.g., $K_u = u'_{RMS} L_E$). The time-ensemble median, 25%, and 75% quantiles were chosen to summarize K for each burst.

Tracer Addition

[13] An NDS, consisting of six lengths of irrigation tubing designed to release water at a constant rate (2 L h^{-1}) through each exit port (spaced ~0.2 m apart) when under pressure by a small submersible pump placed within a 50-L holding tank, was placed perpendicular to the main flow direction upstream of the *C. nodosa* leading edge at $x = -2$ m (Fig. 2). Lines of irrigation tubing were positioned at $h = 0.15$, 0.3, 0.45, 0.6, 0.75, and 0.9 m, across a distance of 5 m (representing a y–z labeling plane of 3.75 m^2), resulting in an estimated tracer releases rate of 0.05 m h^{-1}. The first line of tubing was 5 cm above the top of the *C. prolifera* canopy.

[14] Using a priori information about the water velocity, the delivery rate of the tracer, and water column NH_4^+ concentration, we added 25 g of $^{15}NH_4Cl$ ($x(^{15}N) = 98\%$) to the holding tank (for recent recommendations on stable-isotope terminology, see Coplen 2011) to increase in situ water column ^{15}N concentration by ~5%. However, actual dilution of the $^{15}NH_4^+$ label in the water column was quantified using the fluorescent dye uranine (an Na salt of fluorescein; $C_{20}H_{10}Na_2O_5$, M = 376.28 g mol^{-1}, Flury and Wai 2003). The uranine concentration recovered in the water column varied between 1.2 and 28.5 μg L^{-1}.

[15] Labeling of the water column was initiated by filling two 50-L containers with seawater from the site and, shortly before pumping the mixture through the NDS, spiking them each with 1 L concentrated tracer and thoroughly mixing. Pumping of the mixture continued for 30 min and did not completely empty the containers, resulting in a total volume discharged of ~90 L.

[16] A water collection system, consisting of 28 tubes connected to two peristaltic pumps, was positioned to collect water samples at $x = -1$, −0.5, 0, 0.5, 1, 2, and 4 m and heights of $h = 0.15$, 0.3, 0.5, and 1 m (Fig. 2). Thus, samples were collected 5 cm above the *C. prolifera* canopy, as well as within and above the *C. nodosa* canopy. Water samples (20 ml) were collected at 5, 10, 20, 30, and 40 min from the start of tracer release and immediately stored on ice within a cool box. Sampling times were corrected for the time required for water to travel to the boat via the tubing (~2 min).

Chemical and Isotopic Analysis

[17] Before the nutrient release, 9, 17, and 3 samples (0.5 gDM) of *C. prolifera*, *C. nodosa*, and the unattached macroalgae *Gracilaria* sp., respectively, were collected haphazardly from the experimental area for natural abundance stable-isotope analysis. At the end of the labeling period (40 min), divers carefully collected biomass samples by hand of *C. prolifera*, *C. nodosa*, and *Gracilaria* sp. (depending on their occurrence) from four 0.2 × 0.2–m plots situated next to each of the water collection points (Fig. 2).

[18] Samples were stored in a cool box until they were transported to the laboratory (within 4 h). No obvious epiphytes could be observed on *C. prolifera*. Epiphytes on the leaves of *C. nodosa* were removed by carefully scraping with a razor blade, stored on preashed GF/C glass fiber filters (Whatman, UK), and freeze-dried. Macrophyte tissues were separated from the sediment, cleaned in seawater, washed briefly with distilled water, and separated into above-sediment (assimilators, leaves, and sheath) and below-sediment (rhizoids, rhizome, and roots) parts before being freeze-dried and ground to a fine powder.

[19] Dried samples of macrophyte tissues and epiphytes were analyzed using an elemental analyzer (Thermo EA 1112, Thermo Fisher Scientific, USA) coupled to an isotope ratio mass spectrometer (Thermo Delta V Advantage, Thermo Fisher Scientific) with a Conflo II interface (elemental analyzer-isotopic ratio mass spectrometer), allowing determination of nitrogen and carbon content (μmol $(gDM)^{-1}$) and ^{15}N atomic fractions of dry matter ($x(^{15}N)_{DM}$).

[20] The uranine concentration (μg L^{-1}) within unfiltered water samples was measured using a fluorometer (TD-700, Turner Designs, USA) fitted with fluorescein excitation (490 nm) and emission (580 nm) filters and a blue mercury lamp (kit 10-086R). Ammonium concentrations of filtered (GF/F filter, Whatman) water samples collected upstream of the NDS were analyzed colorimetrically.

Calculations and Statistics

[21] Downstream uranine and upstream NH_4^+ concentrations were used to estimate the ^{15}N atomic fraction of the water column ($x(^{15}N)_{aq.N}$) during the labeling period, that is, the actual dilution of the $^{15}NH_4^+$ label. Weighted-mean uranine concentration (weighted by the time interval 0–40 min; see below) was fitted to a second-order polynomial surface (x–z; see below), and uranine values were extracted at each x-position corresponding to the respective heights of the macrophytes. These regions were defined as the top of the *C. prolifera* canopy, within the *C. nodosa* canopy, 0.05 m above the sediment surface for *Gracilaria* sp., and the top of the *C. nodosa* canopy for epiphytes. Concentrations of added NH_4^+ (μmol $NH_4^+L^{-1}$) were calculated as

$$[NH_4^+]_{tracer} = \text{uranine concentration} \times M_{tracer}/\text{at.wt.}_{NH_4Cl}, \quad (1)$$

where M_{tracer} is the mass ratio of $^{15}NH_4Cl$:uranine of the initial tracer mix (1.67 g g^{-1}) and at.wt._{NH_4Cl} is the atomic weight of ammonium chloride (54.5).

[22] The ^{15}N atomic fraction of the dissolved N source pool in the water column ($x(^{15}N)_{aq.N}$) was then calculated as

$$x(^{15}N)_{aq.N} = \frac{([NH_4^+]_{tracer}x(^{15}N)_{tracer}) + ([NH_4^+]_{water}x(^{15}N)_{initial})}{[NH_4^+]_{tracer} + [NH_4^+]_{water}}, \quad (2)$$

where $x(^{15}N)_{tracer}$ is the atomic fraction of the added tracer (0.98), $[NH_4^+]_{water}$ is 10.6 ± 3.5 μmol-$NH_4^+L^{-1}$ (mean ± SE), and $x(^{15}N)_{initial}$ is the atomic fraction of the initial water column (estimated as the mean atomic fraction of all macrophyte above-sediment natural abundance tissue samples, 3.68×10^{-3}).

[23] Excess atom fractions ($x^E(^{15}N)_{DM\_sample}$) were calculated as the difference between the atomic fraction labeled ($x(^{15}N)_{DM\_sample}$) and natural abundance $x(^{15}N)_{DM\_nat.ab}$) of plant dry matter samples (Van Engeland et al. 2011). Dry-matter-specific uptake rates of NH_4^+ ($V_{sample}(NH_4^+)$, μmol NH_4^+ $gDM^{-1}h^{-1}$) were calculated as

$$V_{sample}(NH_4^+) = \left(\frac{x^E(^{15}N)_{DM\_sample}}{x(^{15}N)_{aq.N} \times t}\right) \times [N]_{DM\_sample}, \quad (3)$$

where $[N]_{DM\_sample}$ is the tissue nitrogen content (μmol-N gDM^{-1}) and t is the length of exposure to the tracer (0.67 h).

[24] These calculations assume that variations in water column NH_4^+ concentration, depletion by biological activity, and isotope dilution due to regeneration were minimal within the labeling area. Furthermore, it is assumed that $x(^{15}N)_{initial}$ was similar to the natural abundance of the community of macrophytes, which is supported by previous studies (Morris et al. 2009). To help assess assumptions about N depletion and dilution of the water column NH_4^+ source pool by uptake and regeneration, respectively, areal uptake rates (μmol NH_4^+m-benthos$^{-2}h^{-1}$) were calculated by multiplying $V_{sample}(NH_4^+)$ at each x-position by the areal biomass (gDM m^{-2}) of each tissue component

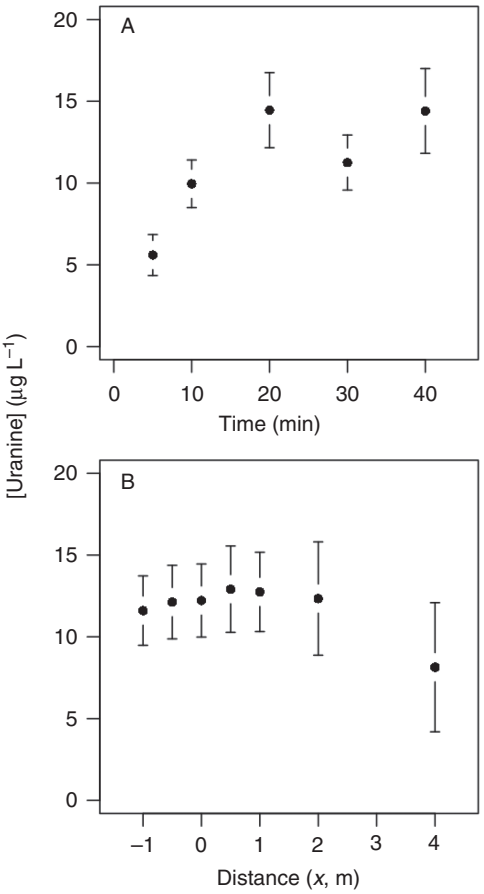

Fig. 3 Depth-averaged uranine concentrations (weighted mean ±95% confidence interval) grouped by time (A) and x-position (B). Pumping of label ceased after 30 min.

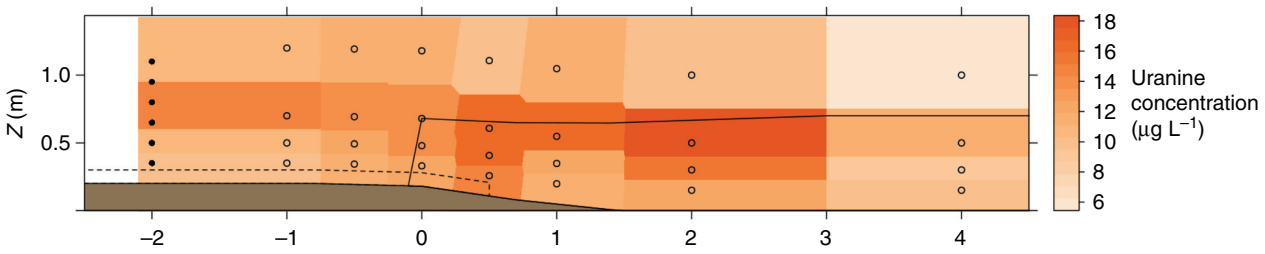

Fig. 4 Weighted mean uranine concentration during the labeling period (0–45 min). Other details are as in Fig. 2A.

and integrating over the study area to provide an estimate of the potential areal uptake rate of the community. Examples of the magnitude of benthic NH_4^+ regeneration rates were derived from Fulweiler et al. (2010) and Mortazavi et al. (2012).

[25] Statistics were performed with the statistical program R 2.15 (R Core Team 2013). Significant isotope excesses were assessed using nonparametric Kruskal–Wallis rank sum tests (kruskal.test function) and nonparametric multiple test procedures (Behrens–Fisher, Satterthwaite *t*-approximation; npmc function) to examine differences between natural abundance and labeled sample atomic fractions. The same tests were used to examine differences between uptake rates at different positions for each biological component and to examine differences between components. Significance levels were set at $p < 0.05$. Uranine and water velocity data were fitted to a second-order-polynomial surface by using the function surf.ls (Venables and Ripley 2002). Pearson's product-moment correlation was used to test for significant correlation between water velocity and specific uptake (cor.test function). Error propagation (Monte Carlo simulations) calculations for areal uptake values were carried out using the function propagate (Ritz and Spiess 2008).

Results

[26] The spatially (x–z) weighted-mean uranine concentration reached a steady value of ~15 μg L^{-1} after 15 min of labeling (Fig. 3A). Time- and z-weighted mean uranine concentration was relatively homogeneous in the x-direction, although slightly lower values were recorded at $x = 4$ m (Fig. 3B). This could be mainly attributed to differences in the vertical distribution of the tracer over time (Fig. 4); time-weighted mean uranine concentration during the labeling period (0–45 min) ranged from a maximum of 17.6 μg L^{-1} observed at the top of the *Cymodocea nodosa* canopy at $x = 2$ m to a minimum of 6.2 μg L^{-1} in the upper water column at $x = 4$ m. However, the lowest uranine concentration corresponding to a depth region with uptake measurements was 8.7 μg L^{-1} at the sediment surface, $x = -1$ m. Thus, effective $^{15}NH_4^+$ tracer concentrations were between 0.27 and 0.47 μmol $NH_4^+ L^{-1}$ (an increase in total water column $[NH_4^+]$ of between 2.5% and 4.5%), which represented an increase of ^{15}N ($x(^{15}N)_{aq.N}/x(^{15}N)_{initial} \times 100$) of between 650% and 1130%.

[27] Free-stream water velocity ($(\bar{u})$ at $z = 1.08$ m) was 0.040 ± 0.005 m s^{-1} (mean ± SD; Fig. 5A). Vertically averaged $\bar{u}$ within the *C. nodosa* canopy was 0.017 ± 0.004, 0.019 ± 0.012, and 0.025 ± 0.009 m s^{-1} at $x = 0$, 0.69, and 1.46 m, respectively, suggesting that velocities increased up to a distance of at least 1.5 m from the leading edge. Root-mean-squared velocity deviations (u'_{RMS}) ranged between 0.007 and 0.028 m s^{-1} and appeared relatively similar between profiles (Fig. 5A, error bars). As expected, w'_{RMS} values were much smaller than in the x-direction, apart from at $x = 1.46$ m (Fig. 5B, error bars), where values as high as 0.014 m s^{-1} were observed near the *C. nodosa* canopy interface.

[28] Median turbulent diffusivity coefficients (K) in the x- and y-directions were similar (K_x and K_y were 1.08×10^{-2} and 8.91×10^{-3} m^2 s^{-1}, respectively) and about three times larger than vertical diffusivity ($K_z = 2.99 \times 10^{-3}$ m^2 s^{-1}). Vertical profiles of diffusivity showed similar tendencies in the x-, y-, and z-directions

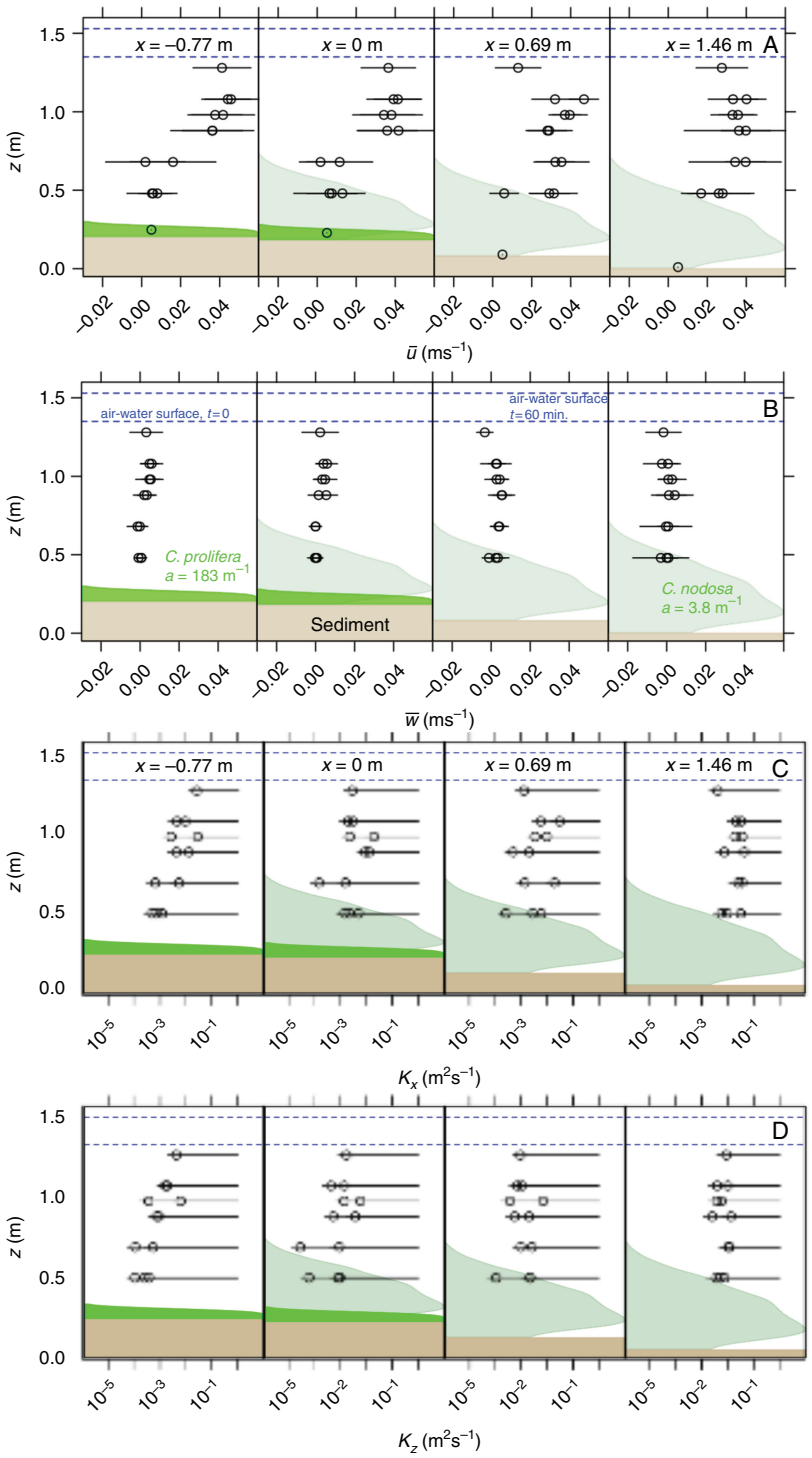

Fig. 5 Profiles of horizontal (A) and vertical velocity (B) and horizontal (C) and vertical turbulent diffusivity (D) measured during 1–3 bursts of 300 s depending on height at $x = -0.77$, 0, 0.69, and 1.46 m. Schematics of relative sediment, canopy, and water level positions are shown as in Fig. 2 at $x = -0.77$, 0, 0.69, and 1.46 m. Error bars represent root-mean-squared velocity deviations and quantiles (25% and 75%) for velocities and turbulent diffusivity, respectively. Dashed blue lines represent the air–water interface at the start (1.35 m) and end (1.53 m) of the experiment. Green polygons represent the relative vertical distribution of frontal surface area per water volume (a/a_{max}) of the *C. prolifera* (bright green) and *C. nodosa* (transparent dark green) canopies. Vertically integrated a for each canopy is shown as text. Brown polygons represent the sediment height. Water column height (z-position, m) is relative to the sediment surface at $x = 2$ m.

Table 2 Summary of specific uptake rates, biomass, and areal uptake for each of the community components under natural hydrodynamic conditions ($u_{z=1\,m} = 0.04\,m\,s^{-1}$) [mean ± SD (*n*)]. Incubation time was 0.67 h, and in situ [NH_4^+] was 11 μmol L^{-1}. Superscript letters highlight significantly different specific uptake rates (Behrens–Fisher test, $p < 0.05$). Biomass estimates for *Gracilaria* sp. and *C. nodosa* roots were unavailable.

Component	Uptake (μmol NH_4^+ $gDM^{-1}\,h^{-1}$)	Biomass (gDM m^{-2})	Areal uptake (μmol $NH_4^+\,m^{-2}\,h^{-1}$)
Cymodocea nodosa epiphytes	16.58 ± 11.47[a] (23)	46 ± 23 (4)	762 ± 699
Cymodocea nodosa leaf	4.10 ± 1.99[b] (23)	258 ± 50 (4)	1055 ± 559
Caulerpa prolifera above sediment	3.85 ± 2.88[b] (16)	200 ± 25 (4)	772 ± 590
Gracilaria sp.	1.01 ± 1.72[c] (13)		
Cymodocea nodosa root	0.29 ± 0.30[c] (23)		

(Fig. 5C–D); values decreased toward the canopy at $x = -0.77$ m, whereas they were higher and relatively constant throughout the water column at $x = 1.46$ m. Profiles at the patch edge ($x = 0$ and 0.69 m) appeared to be intermediate between these two situations. This resulted in significantly different water column K_z values among positions (Kruskal–Wallis rank sum test, $\chi^2_{(3,48)} = 21.6$, $p < 0.001$), with values at $x = 1.46$ m ($0.01\,m^2\,s^{-1}$) much higher than the other positions ($0.002\,m^2\,s^{-1}$; Behrens–Fisher test, $p < 0.05$). This effect could be attributed to an increase in both w'_{RMS} (see above) and L_{E_z}; L_{E_z} was 1.78 m at $x = 1.46$ m and 0.47 m at the other positions ($p < 0.05$).

[29] Significant increases in $x(^{15}N)_{DM\_sample}$ compared to $x(^{15}N)_{DM\_nat.ab}$ (data not shown) were observed for *C. nodosa* leaves (Kruskal–Wallis rank sum test, $\chi^2_{(6,33)} = 31.1$, $p < 0.001$), *C. nodosa* epiphytes ($\chi^2_{(6,31)} = 30.0$, $p < 0.001$), and *C. prolifera* above-sediment tissues ($\chi^2_{(4,20)} = 18.1$, $p < 0.01$). Nonparametric multiple test procedures revealed that all labeling positions showed significant uptake of ^{15}N for *C. nodosa* leaves and epiphytes (Behrens–Fisher test, $p < 0.05$), and only a single position of *C. prolifera* above-sediment tissues did not show significant uptake ($x = -1$ m).

[30] Mean specific NH_4^+ uptake rates of the macrophyte community components ranged from a minimum of 0 (i.e., no significant uptake, see above) to a maximum of 25.0 μmol NH_4^+ $gDM^{-1}\,h^{-1}$ (Fig. 6; only significant uptake of the major components is shown). No differences in the uptake rates at different *x*-positions were found for *C. nodosa* epiphytes or leaves, whereas distance significantly affected the uptake of *C. prolifera* above-sediment tissues (Kruskal–Wallis rank sum test, $\chi^2_{(2,9)} = 31.1$, $p < 0.05$), with uptake at $x = 0.5$ m higher than at $x = 0$ and −0.5 m (Behrens–Fisher test, $p < 0.05$).

[31] When specific uptake rates were pooled per component, *C. nodosa* epiphytes had the highest uptake; no significant differences where found between *C. nodosa* leaves and *C. prolifera* above-sediment, and *Gracilaria* sp. and *C. nodosa* roots had the lowest rates of uptake (Table 2; Behrens–Fisher test, $p < 0.05$). Upscaling suggested that even though *C. nodosa* leaves had uptake rates four times lower than those of epiphytes, because of their high biomass they were the dominant component in terms of areal uptake (Table 2). When considered as a community, the seagrass habitat had an areal uptake rate 2.4 times higher than the *Caulerpa* habitat. Integrating areal uptake for both habitats over the whole study area (6 m × 1 m) suggested that at the in situ NH_4^+ concentration of 10.6 μmol $NH_4^+\,L^{-1}$, vertically averaged longitudinal velocity (U_b) of 0.03 m s^{-1}, and depth of 1.45 m, depletion of total NH_4^+ within a packet of water passing through the study area would be <1% of the ambient concentration. Likewise, based on reported estimates of sediment NH_4^+ regeneration fluxes to the water column (~100–300 μmol $NH_4^+\,m^{-2}\,h^{-1}$; Fulweiler et al. 2010; Mortazavi et al. 2012), dilution of the total-NH_4^+ source pool within a packet of water passing through the study area is not likely to be significant. Ammonium mass transfer coefficients (k_{NH_4}), that is, areal uptake divided by water column NH_4^+ concentration, were 4.76×10^{-5} and $2.02 \times 10^{-5}\,m\,s^{-1}$ for the *C. nodosa* and *C. prolifera* habitats, respectively.

Discussion

[32] This study is one of the first attempts to measure in situ, specific NH_4^+ uptake rates of benthic macro-

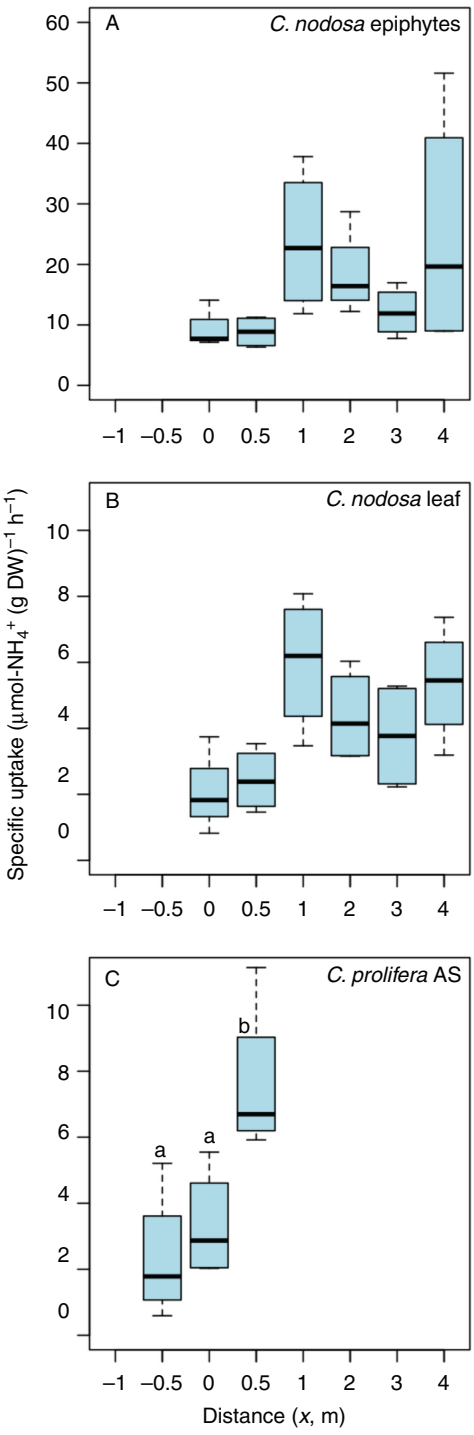

Fig. 6 Specific nitrogen uptake rates at distances relative to the leading edge of a *C. nodosa* patch for *C. nodosa* epiphytes (A), *C. nodosa* leaf (B), and *C. prolifera* above sediment (C). *Gracilaria* sp. and *C. nodosa* roots are not shown. *C. prolifera* was present only at positions −1 to 0.5 m, and *C. nodosa*, at 0–4 m. Significant differences (Behrens–Fisher test, $p < 0.05$) in *C. prolifera* uptake are indicated by different letters. Note that the *y*-axis for epiphytes has a different scale.

phytes and their associated phototrophic community under natural, undisturbed flow conditions. Uptake rates of *Cymodocea nodosa* leaves (collected from the same area) matched well with measurements made at a free stream velocity of 0.05 m s^{-1} in a flow chamber (3.57 ± 0.8 µmol NH_4^+ gDM_{leaf}^{-1} h^{-1}; Morris et al. 2008). Ammonium mass transfer coefficients (k_{NH_4}) for the *C. nodosa* (4.76×10^{-5} m s^{-1}) and *Caulerpa prolifera* (2.02×10^{-5} m s^{-1}) habitats were similar to values derived by Cornelisen and Thomas (2009) ($k_{NH_4} = 0.00038\ U_b^{0.69}$, k_{NH_4} (for $U_b = 0.03$) $= 3.38 \times 10^{-5}$ m s^{-1}). Overall, uptake rates measured in this study fall within the range of reported values for seagrasses (Touchette and Burkholder 2000; Alexandre et al. 2011; Van Engeland et al. 2013), epiphytes (Cornelisen and Thomas 2002; Van Engeland et al. 2013), and macroalgae (Hein et al. 1995; Malta et al. 2005; Van Engeland et al. 2013).

[33] Clear differences in flow properties were observed at the transition between canopy types. Hydrodynamic measurements suggested that longitudinal advection, as well as turbulent diffusivity, increased within the *C. nodosa* bed (Fig. 5). Vertically averaged $\bar{u}$ within the *C. nodosa* canopy was 0.017 ± 0.004, 0.019 ± 0.012, and 0.025 ± 0.009 m s^{-1} at $x = 0$, 0.69, and 1.46 m, respectively, and K_z at $x = 1.46$ m (0.01 m^2 s^{-1}) was much higher than the other positions (0.002 m^2 s^{-1}). Hence, the prediction that flow over the transition between the dense *C. prolifera* canopy and the sparse *C. nodosa* canopy will lead to an acceleration of near-bed water velocities appears to be reasonable. The vertical profile at $x = -0.77$ m and a similar pattern in the profile at $x = 0$ m also suggest that flow adjustment began at length scale comparable to the *C. nodosa* canopy height (0.5–0.7 m) upstream of the leading edge. However, despite these longitudinal differences in hydrodynamic properties, we were unable to detect significant longitudinal variation in specific uptake for *C. nodosa* leaves or epiphytes (Fig. 6). This was probably a consequence of the relatively small differences in flow velocity, resulting in small observable effects on uptake compared with the high within-replicate variability of measurements. Higher uptake rates of *C. prolifera* at the boundary ($x = 0.5$ m) compared with upstream of the *C. nodosa*

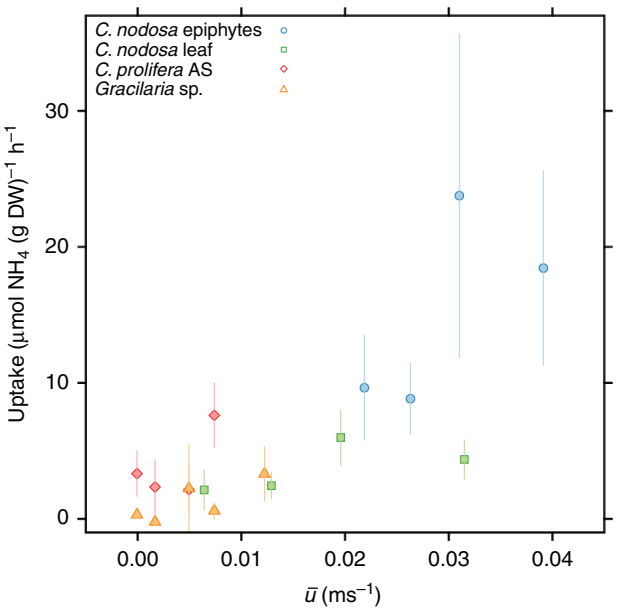

Fig. 7 Specific nitrogen uptake rates (mean ± SD) plotted against time-ensemble mean water velocity ($\bar{u}$, m s^{-1}) at the depth region corresponding to each community component between $x = -1$ and 2 m (see text for details). Water velocities corresponding to the position of each component were extracted from an interpolation of vertical profiles collected at $x = -0.77$, 0, 0.69, and 1.46 m.

patch were observed, suggesting a possible mechanism that may favor the expansion of *C. prolifera*; however, this effect was difficult to assess because of incomplete mixing of the tracer close to the release point (i.e., no significant uptake at $x = -1$ m).

[34] In contrast, the relatively larger variations in vertical velocity experienced by biotic components of the community at different heights above the bed indicate that water velocity is a relatively good predictor of uptake (Fig. 7). By modeling $\bar{u}$ at the corresponding x–z coordinates for each community component where uptake measurements were collected, we can see that specific uptake was significantly correlated with $\bar{u}$ (Pearson's product-moment correlation, $r = 0.78$, $t_{15} = 4.9$, $p < 0.001$). Hence, the higher uptake rates of epiphytes can be explained by their elevated position on the surface of leaves extending into the faster-flowing region at the top of the canopy. Likewise, the lack of significant uptake by *Gracilaria* sp. was probably related to its vertical position within the lower canopy of the *C. prolifera* bed where flow velocities (Hendriks et al. 2010) and vertical diffusivity are low (Nepf and Ghisalberti 2008).

[35] The relative contributions of longitudinal advection and turbulent diffusion in determining mass transport can be summarized by comparing their respective time scales, L_x/U_b and L/K, using the dimensionless turbulent Péclet number, $Pe = U_b L^2/KL_x$, where $U_b = 0.03$ m s^{-1}, L_x is the characteristic length scale of the *C. nodosa* patch (4 m), and L is a characteristic length scale for diffusion. Considering the sampling area and the mean canopy height of the *C. nodosa* patch as the characteristic length scales ($x = 4$ m, $y = 2$ m, and $z = 0.6$ m) gives *Pe* values in the *x*-, *y*-, and *z*-directions of 11, 3.5, and 0.9, suggesting that advection dominates longitudinal and lateral patch-scale transport. This observation is consistent with that of Lara et al. (2012), who estimated similar lateral K (between 1 and 5×10^{-3} m^2 s^{-1}) and $Pe > 1$ in adjacent seagrass communities by using independent techniques. At the scale of the *C. nodosa* canopy height vertical *Pe* is close to 1, suggesting that neither process is dominant. Taking a length scale of 0.1 m (i.e., *C. prolifera* canopy height), vertical *Pe* is $<<1$ suggesting that the contribution of turbulent diffusion to mass transport is much larger for the *C. prolifera* canopy.

Significance to Aquatic Environments

[36] The labeling of a submerged *Caulerpa prolifera*–*Cymodocea nodosa* landscape in the field with a mix of $^{15}NH_4^+$ and uranine enabled the measurement of in situ specific NH_4^+ uptake rates of benthic macrophytes and their associated phototrophic community under undisturbed flow. The transition from a *C. prolifera* to a *C. nodosa* bed included both a change in benthic canopy properties (short and dense to tall and sparse) and sediment topography (0.2 m increase in water column depth) that resulted in an increase in longitudinal advection and turbulent diffusivity within the *C. nodosa* canopy between 0.5 and 1.5 m from the leading edge. Nevertheless, we were unable to clearly identify significant longitudinal differences in N uptake rates. However, vertical differences in flow velocities related to the position of organisms (i.e., near the top vs. near the bottom of the canopy) appeared to be a good indicator of uptake. These results highlight the important role that hydrodynamics plays in controlling the transport of nutrients to the benthos and how the interplay

between the physical structure of organisms and flow within the benthic boundary layer may determine the nutrient transport niches of individual species within macrophyte communities. Interpretations and models of macrophyte ecosystem functioning should incorporate the spatial heterogeneity created through the interaction of canopy morphology, bathymetry, and hydrodynamics.

Acknowledgments This research was supported by regional government of Andalusia project FUNDIV ("Functional diversity of submerged macrophytes: Influence on carbon and nitrogen processing") (P07-RNM-2516), the Spanish project IMACHYDRO ("Interactions between marine macrophyte beds and hydrodynamics: From organisms to ecosystems" CTM2008-00012/MAR), a travel grant from the Schure-Beijerinck-Popping Fund (SBP/JK/2007-32), and the Netherlands Organization for Scientific Research. Thanks to P. García-Marin and I. Hernandez (Project EcoLagunes (Environmental Management of Aquaculture Achievement Wetlands), INTERREG-SUDOE-SOE1/P2/F153) for supplying epiphyte biomass values, Fidel Echevarría Navas (director of Centro Andaluz de Ciencia y Tecnología Marinas) for granting us access to facilities, to Bas Koutstaal for helping with sample processing, and to L. Del Río Rodríguez for supplying aerial photographs. E.P.M. is presently supported by a Junta para la Ampliación de Estudios (JAE-Doc-2010) contract, funded in part by the European Union (European Social Fund, ESF2007-2013) and the Spanish Ministry for Economy and Competitiveness. This is CEIMAR journal publication no. 34.

References

Ackerman, J. D., and A. Okubo. 1993. Reduced mixing in a marine macrophyte canopy. Funct. Ecol. **7**: 305–309. doi:10.2307/2390209.

Alexandre, A., J. Silva, T. J. Bouma, and R. Santos. 2011. Inorganic nitrogen uptake kinetics and whole-plant nitrogen budget in the seagrass *Zostera noltii*. J. Exp. Mar. Biol. Ecol. **401**: 7–12. doi:10.1016/j.jembe.2011.03.008.

Alvarez, O., B. Tejedor, L. Tejedor, and B. A. Kagan. 2003. A note on sea-breeze-induced seasonal variability in the K1 tidal constants in Cádiz Bay, Spain. Estuar. Coast. Shelf Sci. **58**: 805–812. doi:10.1016/S0272-7714(03)00186-0.

Bilger, R. W., and M. J. Atkinson. 1992. Anomalous mass transfer of phosphate on coral reef flats. Limnol. Oceanogr. **37**: 261–272. doi:10.4319/lo.1992.37.2.0261.

Bouma, T. J., M. B. De Vries, E. Low, G. Peralta, C. Tanczos, J. Van de Koppel, and P. M. J. Herman. 2005. Trade-offs related to ecosystem engineering: A case study on stiffness of emerging macrophytes. Ecology **86**: 2187–2199. doi:10.1890/04-1588.

Coplen, T. B. 2011. Guidelines and recommended terms for expression of stable-isotope-ratio and gas-ratio measurement results. Rapid Commun. Mass Spectrom. **25**: 2538–2560.

Cornelisen, C. D., and F. I. M. Thomas. 2002. Ammonium uptake by seagrass epiphytes: Isolation of the effects of water velocity using an isotope label. Limnol. Oceanogr. **47**: 1223–1229. doi:10.4319/lo.2002.47.4.1223.

Cornelisen, C. D., and F. I. M. Thomas. 2004. Ammonium and nitrate uptake by leaves of the seagrass *Thalassia testudinum*: Impact of hydrodynamic regime and epiphyte cover on uptake rates. J. Mar. Syst. **49**: 177–194. doi:10.1016/j.jmarsys.2003.05.008.

Cornelisen, C., and F. Thomas. 2009. Prediction and validation of flow-dependent uptake of ammonium over a seagrass-hard-bottom community in Florida Bay. Mar. Ecol. Prog. Ser. **386**: 71–81. doi:10.3354/meps08065.

Falter, J. L., M. J. Atkinson, and M. A. Merrifield. 2004. Mass-transfer limitation of nutrient uptake by a wave-dominated reef flat community. Limnol. Oceanogr. **49**: 1820–1831. doi:10.4319/lo.2004.49.5.1820.

Fernandes, M., S. Bryars, G. Mount, and D. Miller. 2009. Seagrasses as a sink for wastewater nitrogen: The case of the Adelaide metropolitan coast. Mar. Pollut. Bull. **58**: 303–308. doi:10.1016/j.marpolbul.2008.10.006.

Flury, M., and N. N. Wai. 2003. Dyes as tracers for vadose zone hydrology. Rev. Geophys. **41**: 1002. doi:10.1029/2001RG000109.

Folkard, A. M. 2005. Hydrodynamics of model *Posidonia oceanica* patches in shallow water. Limnol. Oceanogr. **50**: 1592–1600. doi:10.4319/lo.2005.50.5.1592.

Fonseca, M. S., J. S. Fisher, J. C. Zieman, and G. W. Thayer. 1982. Influence of the seagrass, *Zostera marina* L., on current flow. Estuar. Coast. Shelf Sci. **15**: 351–364. doi:10.1016/0272-7714(82)90046-4.

Fonseca, M. S., and M. A. R. Koehl. 2006. Flow in seagrass canopies: The influence of patch width. Estuar. Coast. Shelf Sci. **67**: 1–9. doi:10.1016/j.ecss.2005.09.018.

Freitas, R., A. M. Rodrigues, E. P. Morris, J. L. Perez-Llorens, and V. Quintino. 2008. Single-beam acoustic ground discrimination of shallow water habitats: 50 kHz or 200 kHz frequency, survey? Estuar. Coast. Shelf Sci. **78**: 613–622. doi:10.1016/j.ecss.2008.02.007.

Fulweiler, R. W., S. W. Nixon, and B. A. Buckley. 2010. Spatial and temporal variability of benthic oxygen demand and nutrient regeneration in an anthropogenically impacted New England estuary. Estuar. Coasts. **33**: 1377–1390. doi:10.1007/s12237-009-9260-y.

Gambi, M. C., A. R. M. Nowell, and P. A. Jumars. 1990. Flume observations on flow dynamics in *Zostera marina* (eelgrass) beds. Mar. Ecol. Prog. Ser. **61**: 159–169. doi:10.3354/meps061159.

Gaylord, B., and M. Denny. 1997. Flow and flexibility. I. Effects of size, shape and stiffness in determining wave forces on the

stipitate kelps *Eisenia arborea* and *Pterygophora californica*. J. Exp. Biol. **200**: 3141–3164.

Ghisalberti, M., and H. Nepf. 2009. Shallow flows over a permeable medium: The hydrodynamics of submerged aquatic canopies. Transp. Porous Media. **78**: 309–326. doi:10.1007/s11242-008-9305-x.

Goring, D. G., and V. I. Nikora. 2002. Despiking acoustic Doppler velocimeter data. J. Hydraul. Eng. **128**: 117–126. doi:10.1061/(ASCE)0733-9429(2002)128:1(117).

Gribsholt, B., et al. 2005. Nitrogen processing in a tidal freshwater marsh: A whole ecosystem ^{15}N labeling study. Limnol. Oceanogr. **50**: 1945–1959. doi:10.4319/lo.2005.50.6.1945.

Hein, M., M. F. Pedersen, and K. Sand-Jensen. 1995. Size-dependent nitrogen uptake in micro-and macroalgae. Mar. Ecol. Prog. Ser. **118**: 247–253. doi:10.3354/meps118247.

Hemminga, M. A., B. P. Koutstaal, J. Soelen, and A. G. A. Merks. 1994. The nitrogen supply to intertidal eelgrass (*Zostera marina*). Mar. Biol. **118**: 223–227. doi:10.1007/BF00349788.

Hendriks, I. E., T. J. Bouma, E. P. Morris, and C. M. Duarte. 2010. Effects of seagrasses and algae of the *Caulerpa* family on hydrodynamics and particle-trapping rates. Mar. Biol. **157**: 473–481. doi:10.1007/s00227-009-1333-8.

Holtappels, M., and A. Lorke. 2011. Estimating turbulent diffusion in a benthic boundary layer. Limnol. Oceanogr. Methods **9**: 29–41. doi:10.4319/lom.2010.9.29.

Hughes, J. E., L. A Deegan, B. J. Peterson, R. M. Holmes, and B. Fry. 2000. Nitrogen flow through the food web in the oligohaline zone of a New England estuary. Ecology **81**: 433–452. doi:10.1890/0012-9658(2000)081[0433:NFTTFW]2.0.CO;2.

Hurd, C. L., P. J. Harrison, and L. D. Druehl. 1996. Effect of seawater velocity on inorganic nitrogen uptake by morphologically distinct forms of *Macrocystis integrifolia* from wave-sheltered and exposed sites. Mar. Biol. **126**: 205–214. doi:10.1007/BF00347445.

Koch, E. W., J. D. Ackerman, J. Verduin and M. van Keulen. 2006. Fluid dynamics in seagrass ecology—from molecules to ecosystems. Pp. 193–225. *In* A. W. D. Larkum, R. J. Orth, and C. Duarte [eds.], Seagrasses: Biology, Ecology and Their Conservation. Springer.

Koch, E. W., and G. Gust. 1999. Water flow in tide- and wave-dominated beds of the seagrass *Thalassia testudinum*. Mar. Ecol. Prog. Ser. **184**: 63–72. doi:10.3354/meps184063.

Lacy, J. R., and S. Wyllie-Echeverria. 2011. The influence of current speed and vegetation density on flow structure in two macrotidal eelgrass canopies. Limnol. Oceanogr. Fluids Environ. **1**: 38–55. doi:10.1215/21573698-1152489.

Lepoint, G., J. Jacquemart, J. M. Bouquegneau, V. Demoulin, and S. Gobert. 2007. Field measurements of inorganic nitrogen uptake by epiflora components of the seagrass *Posidonia oceanica* (Monocotyledons, Posidoniaceae). J. Phycol. **43**: 208–218. doi:10.1111/j.1529-8817.2007.00322.x.

Malta, E. J., D. G. Ferreira, J. J. Vergara, and J. L. Perez-Llorens. 2005. Nitrogen load and irradiance affect morphology, photosynthesis and growth of *Caulerpa prolifera* (Bryopsidales: Chlorophyta). Mar. Ecol. Prog. Ser. **298**: 101–114. doi:10.3354/meps298101.

Maltese, A., E. Cox, A. M. Folkard, G. Ciraolo, G. La Loggia, and G. Lombardo. 2007. Laboratory measurements of flow and turbulence in discontinuous distributions of ligulate seagrass. J. Hydrol. Eng. **133**: 750–760. doi:10.1061/(ASCE)0733-9429(2007)133:7(750).

Morris, E. P., G. Peralta, F. G. Brun, L. Van Duren, T. J. Bouma, and J. L. Perez-Llorens. 2008. Interaction between hydrodynamics and seagrass canopy structure: Spatially explicit effects on ammonium uptake rates. Limnol. Oceanogr. **53**: 1531–1539. doi:10.4319/lo.2008.53.4.1531.

Morris, E. P., et al. 2009. *Caulerpa prolifera* stable isotope ratios reveal anthropogenic nutrients within a tidal lagoon. Mar. Ecol. Prog. Ser. **390**: 117–128. doi:10.3354/meps08184.

Mortazavi, B., A. A. Riggs, J. M. Caffrey, H. Genet, and S. W. Phipps. 2012. The contribution of benthic nutrient regeneration to primary production in a shallow eutrophic estuary, Weeks Bay, Alabama. Estuar. Coasts. **35**: 862–877. doi:10.1007/s12237-012-9478-y.

Naldi, M., and P. Viaroli. 2002. Nitrate uptake and storage in the seaweed *Ulva rigida* C. Agardh in relation to nitrate availability and thallus nitrate content in a eutrophic coastal lagoon (Sacca di Goro, Po River Delta, Italy). J. Exp. Mar. Biol. Ecol. **269**: 65–83. doi:10.1016/S0022-0981(01)00387-2.

Nepf, H., and M. Ghisalberti. 2008. Flow and transport in channels with submerged vegetation. Acta Geophys. **56**: 753–777. doi:10.2478/s11600-008-0017-y.

O'Brien, M. C., and P. A. Wheeler. 1987. Short term uptake of nutrients by *Enteromorpha prolifera* (Chlorophyceae). J. Phycol. **23**: 547–556. doi:10.1111/j.1529-8817.1987.tb04204.x.

Pace, M. L., et al. 2007. Does terrestrial organic carbon subsidize the planktonic food web in a clear-water lake? Limnol. Oceanogr. **52**: 2177–2189. doi:10.4319/lo.2007.52.5.2177.

Peralta, G., L. A. van Duren, E. P. Morris, and T. J. Bouma. 2008. Consequences of shoot density and stiffness for ecosystem engineering by benthic macrophytes in flow dominated areas: A hydrodynamic flume study. Mar. Ecol. Prog. Ser. **368**: 103–115. doi:10.3354/meps07574.

Peterson, C. H., R. A. Luettich, Jr, F. Micheli, and G. A. Skilleter. 2004. Attenuation of water flow inside seagrass canopies of differing structure. Mar. Ecol. Prog. Ser. **268**: 81–92. doi:10.3354/meps268081.

R Core Team. 2013. R: A language and environment for statistical computing. R Foundation for Statistical Computing. http://www.R-project.org.

Ritz, C., and A. N. Spiess. 2008. qpcR: an R package for sigmoidal model selection in quantitative real-time polymerase

chain reaction analysis. Bioinformatics **24**: 1549–1551. doi:10.1093/bioinformatics/btn227.

Rominger, J. T., and H. M. Nepf. 2011. Flow adjustment and interior flow associated with a rectangular porous obstruction. J. Fluid Mech. **680**: 636–659. doi:10.1017/jfm.2011.199.

Rubio, L., A. Linares-Rueda, M. J. Garcıa-Sánchez, and J. A. Fernández. 2007. Ammonium uptake kinetics in root and leaf cells of *Zostera marina* L. J. Exp. Mar. Biol. Ecol. **352**: 271–279. doi:10.1016/j.jembe.2007.07.024.

Rueda, J. L., and C. Salas. 2003. Seasonal variation of a molluscan assemblage living in a *Caulerpa prolifera* meadow within the inner Bay of Cádiz (SW Spain). Estuar. Coast. Shelf Sci. **57**: 909–918. doi:10.1016/S0272-7714(02)00421-3.

Stewart, H. L., and R. C. Carpenter. 2003. The effects of morphology and water flow on photosynthesis of marine macroalgae. Ecology **84**: 2999–3012. doi:10.1890/02-0092.

Thomas, F. I. M., and M. J. Atkinson. 1997. Ammonium uptake by coral reefs: Effects of water velocity and surface roughness on mass transfer. Limnol. Oceanogr. **42**: 81–88. doi:10.4319/lo.1997.42.1.0081.

Thomas, F. I. M., and C. D. Cornelisen. 2003. Ammonium uptake by seagrass communities: Effects of oscillatory versus unidirectional flow. Mar. Ecol. Prog. Ser. **247**: 51–57. doi:10.3354/meps247051.

Thomas, F. I. M., C. D. Cornelisen, and J. M. Zande. 2000. Effects of water velocity and canopy morphology on ammonium uptake by seagrass communities. Ecology **81**: 2704–2713. doi:10.1890/0012-9658(2000)081[2704:EOWVAC]2.0.CO;2.

Thursby, G. B., and M. M. Harlin. 1982. Leaf-root interaction in the uptake of ammonia by *Zostera marina*. Mar. Biol. **72**: 109–112. doi:10.1007/BF00396910.

Touchette, B. W., and J. A. M. Burkholder. 2000. Review of nitrogen and phosphorus metabolism in seagrasses. J. Exp. Mar. Biol. Ecol. **250**: 133–167. doi:10.1016/S0022-0981(00)00195-7.

Van Engeland, T., et al. 2011. Potential uptake of dissolved organic matter by seagrasses and macroalgae. Mar. Ecol. Prog. Ser. **427**: 71–81. doi:10.3354/meps09054.

Van Engeland, T. V., et al. 2013. Dissolved organic matter uptake in a temperate seagrass ecosystem. Mar. Ecol. Prog. Ser. **478**: 87–100. doi:10.3354/meps10183.

Venables, W. N., and B. D. Ripley. 2002. Modern Applied Statistics with S. Springer, doi:10.1007/978-0-387-21706-2.

Verduin, J. J., and J. O. Backhaus. 2000. Dynamics of plant-flow interactions for the seagrass *Amphibolis antarctica*: Field observations and model simulations. Estuar. Coast. Shelf Sci. **50**: 185–204. doi:10.1006/ecss.1999.0567.

Vergara, J. J., M. P. García-Sánchez, I. Olivé, P. García-Marín, F. G. Brun, J. L. Pérez-Lloréns, and I. Hernández. 2012. Seasonal functioning and dynamics of *Caulerpa prolifera* meadows in shallow areas: An integrated approach in Cadiz Bay Natural Park. Estuar. Coast. Shelf Sci. **112**: 255–264. doi:10.1016/j.ecss.2012.07.031.

Vergara, J. J., F. X. Niell, and K. T. Bird. 1997. A dynamic model of transient NH_4^+ assimilation in red algae. Mar. Ecol. Prog. Ser. **148**: 295–307. doi:10.3354/meps148295.

Wahl, T. L. 2003. Discussion of "Despiking Acoustic Doppler Velocimeter Data" by Derek G. Goring and Vladimir I. Nikora. J. Hydrol. Eng. **129**: 484.

Wallentinus, I. 1984. Comparisons of nutrient uptake rates for Baltic macroalgae with different thallus morphologies. Mar. Biol. **80**: 215–225. doi:10.1007/BF02180189.

White, B. L., and H. M. Nepf. 2008. A vortex-based model of velocity and shear stress in a partially vegetated shallow channel. Water Resour. Res. **44**: W01412, doi:10.1029/2006WR005651.

Received: 12 June 2013
Amended: 12 September 2013
Accepted: 15 September 2013